

# Evaluating satellite-based precipitation products for drought monitoring in complex mountainous regions: A case study in Armenia

Hrachya Astsatryan<sup>1</sup>, Rita Abrahamyan<sup>1</sup>, Artur Gevorgyan<sup>2,1</sup>, Hasmik Panyan<sup>2</sup>, Furtado Kalli<sup>3</sup>

<sup>1</sup> Institute for Informatics and Automation Problems of NAS RA, Yerevan, Armenia

<sup>2</sup> Hydrometeorology and monitoring center, Yerevan, Armenia

<sup>3</sup> Centre for Climate Research Singapore, Singapore, Singapore

Corresponding author: Hrachya Astsatryan ([hrach@sci.am](mailto:hrach@sci.am))

## Abstract

Droughts cause danger to human health and socioeconomic development worldwide. The traditional station-based analysis of droughts has limitations. The most relevant is the insufficient spatial resolution of the observations, particularly over mountain topography. This study evaluates the performance of two satellite precipitation products—the Integrated Multi-satellitE Retrievals for Global Precipitation Measurement (IMERG) and the Climate Prediction Center Morphing Method (CMORPH)—for monitoring meteorological droughts in mountainous environments, using the Armenian Highlands as a case study. We focused on a drought event in June 2021, which was the hottest and driest month in Armenia in nearly nine decades. The performance of gridded global precipitation products was evaluated against in-situ observations for June 2021. Statistical evaluation using the Pearson correlation coefficient, root mean square error, mean absolute error, mean bias, and standard deviation has been analyzed. Results indicate that both products have challenges in accurately estimating the Standardized Precipitation Index (SPI) under severe drought conditions. However, IMERG's drought detection aligned more closely with in-situ observations than CMORPH's, which tended to underestimate drought severity. In addition to precipitation-based indices, Landsat-8 and Sentinel-2 vegetation and moisture indices (NDVI, NDMI, NDWI) were evaluated, yielding complementary data regarding the impact of drought on the environment. We found a correlation between low SPI values and stressed vegetation (low NDVI/NDMI), validating the ecological impact of the meteorological drought. Outcomes discuss the merits and disadvantages of satellite precipitation records over mountainous regions and advise operational drought monitoring and early warning systems within data-limited topographically complex areas worldwide.

**Key words:** CMORPH, IMERG, in-situ observations, Sentinel-2, Landsat-8, vegetation and drought indices



Academic editor: Gabriela Adina

Moroşanu-Mitoşeriu

Received: 25 August 2025

Accepted: 25 November 2025

Published: 10 February 2026

**Citation:** Astsatryan H, Abrahamyan R, Gevorgyan A, Panyan H, Kalli F (2026) Evaluating satellite-based precipitation products for drought monitoring in complex mountainous regions: A case study in Armenia. Journal of the Bulgarian Geographical Society 54: 93–116. <https://doi.org/10.3897/jbgs.e169740>

Copyright: © Hrachya Astsatryan et al. This is an open access article distributed under terms of the Creative Commons Attribution License (Attribution 4.0 International – CC BY 4.0).

## 1. Introduction

Enhanced land surface temperatures and evapotranspiration, which increase aridity, led to more severe and frequent droughts over the globe in recent decades (Wang et al. 2017). But interlinkages among various types of droughts

exist, and one tends to produce or exacerbate the others. For example, meteorological drought often leads to hydrological and agricultural drought (Wang et al. 2016). Much attention has been given to the studies of climate change impacts in the past decade, including the effects of temperature and precipitation changes on the severity of droughts (Easterling et al. 2007; Spinoni et al. 2017). These studies are critical for a better understanding of the negative impacts of climate change. The imbalance of precipitation–evapotranspiration leads to extreme droughts. Droughts and heat waves considerably influence physical, chemical, and biological systems and can cause socioeconomic stresses (Yao et al. 2018). For example, Southeast Asia and Eurasia have been associated with more intense, frequent, long-lasting, and large-scale droughts during the past few decades (Shi et al. 2020; UNESCAP 2020; Astsatryan et al. 2021). The changes have adverse effects such as reduced agricultural output, water shortage, higher danger of wildfires, degradation of ecosystems, and enhanced pressure on public health and local economies.

Drought can be a natural disaster causing severe socioeconomic and ecological losses (Ahmadalipour and Moradkhani 2018; Zhang et al. 2019). Therefore, monitoring and evaluating droughts reliably and effectively is critical. Traditionally, drought indices are calculated using observational data taken from surface meteorological stations. However, meteorological stations have sparse and uneven spatial distributions, which can give rise to inadequate representations of the spatial features of droughts. Precipitation is characterised by higher spatial and temporal variability than other meteorological parameters such as temperature (Tao et al. 2016; Sun et al. 2018). When the in-situ precipitation data are sparse, the drought indices calculated from the station-observed data usually cannot reflect the drought information of the entire area (Duan et al. 2016; Wu et al. 2018). In recent decades, with the rapid development of remote sensing, global precipitation data products have emerged that can fill gaps in the ground-based observations (Zhong et al. 2019).

Global precipitation datasets are readily available and provide essential information about regions with sparse observational networks. Gridded datasets help investigate climate change and variability (Sen Roy and Balling 2004). For large-scale hydrological and climatological studies, satellites and reanalyses provide rainfall estimates with complete global coverage at a high spatiotemporal resolution. However, since satellite-based datasets are indirect approximations of precipitation, they frequently contain biases and errors. Similarly, reanalyses are based on models with limited representations of precipitation processes, making their precipitation estimates much more uncertain than better-constrained meteorological variables such as winds or temperatures.

For instance, previously it was discovered that European Centre for Medium-Range Weather Forecasts-based global precipitation products, such as ERA-Interim and ERA5, possess large errors in simulating orographic precipitation over mountainous terrain such as the Armenian Highlands, particularly during summer (Gevorgyan 2013, 2018). Similarly, other studies have shown that satellite-based rainfall products such as the Tropical Rainfall Measuring Mission (TRMM) and Integrated Multi-satellite Retrievals for Global Precipitation Measurement (IMERG) tend to under-/overestimate rainfall heavily over complex terrains and arid to semi-arid regions due to their inability to capture convective storms and orographic enhancement (Toté et al. 2015; Ageet et al. 2022).

CMORPH (Climate Prediction Center Morphing Technique) satellite precipitation products have broad application prospects (Zeweldi and Gebremichael 2009). The studies by Xu et al. (2014) showed a strong positive correlation between the station observation data and the precipitation area of CMORPH in China. Wang et al. (2018) estimated the relevance of CMORPH remote sensing precipitation products in Shaanxi Province, China. They found that CMORPH data can reproduce the spatial distribution of annual precipitation in Shaanxi Province. Lu et al. (2018) adopted the Standardized Precipitation Index (SPI) and CMORPH products to capture typical drought events in China. Zhu et al. (2019) found that the IMERG had higher accuracy in capturing drought characteristics over the Xiangjiang River of China compared to CMORPH and TRMM multi-satellite precipitation analysis. Li et al. (2024) also clarified the outstanding skill of IMERG for drought monitoring utility over PERSIANN-CDR (Precipitation Estimation from Remotely Sensed Information using Artificial Neural Networks–Climate Data Record), CHIRPS (Climate Hazards Group InfraRed Precipitation), and TRMM multi-satellite precipitation analysis.

June 2021 was the hottest and driest in Armenia from 1935 to 2022 (Azizyan et al. 2023). The monthly temperature was 4.2°C higher than the norm of 1961–1990 (13.4°C), and precipitation was 27% of the norm (71 mm). The extreme anomalies in temperature and precipitation motivated us to investigate the drought conditions in Armenia using satellite-based precipitation products. The Sixth Assessment Report of the Intergovernmental Panel on Climate Change provided a separate analysis for climate change impact on mountains (Adler et al. 2022), highlighting that mountains are more vulnerable to climate change and climate extremes such as droughts, floods, etc. Satellite-based precipitation products can fill the gaps in drought monitoring over mountain regions where the observational network is sparse due to logistical issues. However, as already mentioned, the satellite-derived precipitation products have biases which can be significant depending on the complexity of terrain, cloud types producing precipitation, e.g., stratiform or convective, and other factors. Therefore, satellite-based precipitation products must be well validated against ground-based in-situ observations to determine their reliability, particularly in mountainous regions. Armenia, with its complex topography and developing observational network, serves as an ideal case study for a region where such vulnerabilities and data gaps intersect.

In addition to precipitation, we further explored the capabilities of satellite datasets for investigating the impacts of drought on ecosystems, considering vegetation and soil moisture indices such as the Normalized Difference Vegetation Index (NDVI), Normalized Difference Moisture Index (NDMI), and Normalized Difference Water Index (NDWI) obtained from Sentinel-2 and Landsat-8. This study is the first attempt to present a comprehensive analysis of drought conditions over Armenia, considering both in-situ and satellite observations.

The main aim is to evaluate the performance of satellite precipitation data sets while monitoring drought in Armenia's complex mountainous region. Specifically, the study aims to:

- Compare meteorological station measurements with satellite-retrieved precipitation estimates.
- Assess the ability of these products to detect occurrences of drought using the SPI.

- Examine the spatio-temporal drought changes by integrating precipitation-based indices with vegetation and moisture indicators (NDVI, NDMI, NDWI) from Sentinel-2 and Landsat-8.

Such integration facilitates assessing drought development and environmental impacts in mountain regions under scarce data. The rest of this paper is organized into the following sections: Section Materials and methods describe the study area, data sources, and the methodology for evaluating climatic and vegetation indices. Section Results presents the results and statistical analysis. Finally, Section Discussion summarizes the key findings and conclusions.

## 2. Materials and methods

### 2.1. Case study area

The climate of Armenia is relatively dry, with an average annual precipitation of 592 mm. Prolonged meteorological droughts have been shown to reduce the country's water resources by around 20 to 45% (World Bank Group and Asian Development Bank 2021). Approximately 80% of the country is threatened by desertification to various degrees. Located in the country's southwest, Ararat Valley is the most arid region in Armenia. However, Ararat Valley plays a significant role in the country's agriculture. Much of the farmland in this region is irrigated, relying on water from Lake Sevan, the Araks, and Vorotan rivers to support crop production.

Armenia's Fourth National Communication to the United Nations Framework Convention on Climate Change reported an average temperature rise of 1.23°C between 1929 and 2016 and a 10% reduction in average annual precipitation volume from 1935 to 2012. A recent study showed that climate change significantly increased the frequency and intensity of hot extreme temperature indices and heat waves in recent decades over Armenia (Gevorgyan et al. 2025). This increases the drought risks in Armenia. As a landlocked country in the

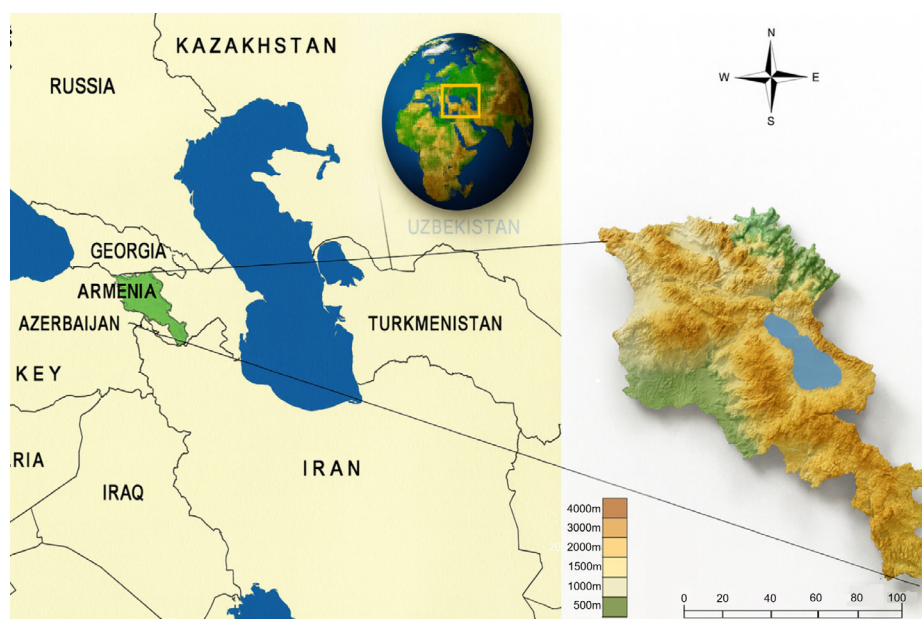


**Figure 1.** Case study area. **A** South Caucasus and Armenian Plateau **B** topography map of Armenia.

Armenian Highlands of West Asia, Armenia borders Turkey to the west, Georgia to the north, Azerbaijan to the east, and Iran to the south. The average elevation of the country is 1,800 m a.s.l., featuring a complex landscape of mountains, valleys, and high plateaus (Fig. 1).

Terrain height is a significant factor affecting climate and precipitation amount in Armenia. Therefore, we defined four elevation zones, which are used for drought analysis in this study. This separation into four zones approximates the dominant topographic gradients of the country, ranging from low valleys to mid-elevation foothills and high plateaus, each having varying regimes of precipitation and vegetation response. Such a stratification enables one to more meaningfully assess how the prevalence of drought varies along the elevation gradient. Fig. 2 presents these elevation zones and the spatial pattern of mean annual precipitation across the country.

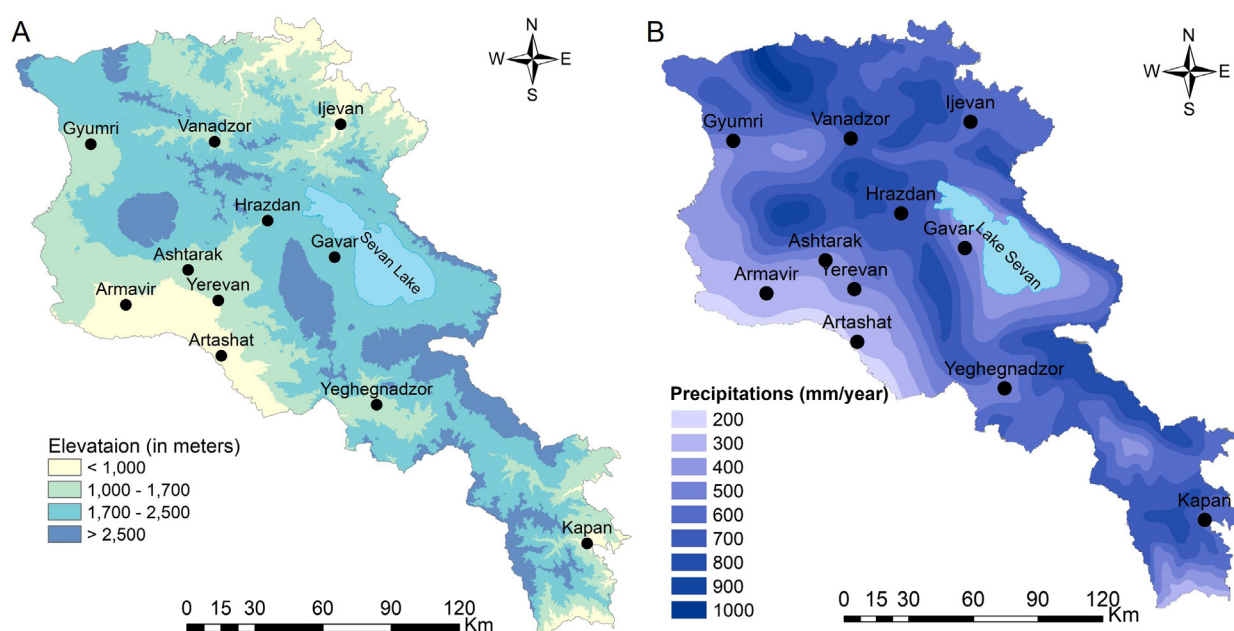


**Figure 2.** Characteristic of the case study area. **A** elevation map of Armenia showing four altitude zones **B** spatial distribution of mean annual precipitation (mm/year).

## 2.2. Datasets

### 2.2.1. Ground-Based Meteorological Observations

The Armenian Hydrometeorology and Monitoring Center (HMC) has a network of meteorological and hydrological observation sites. In this study, 32 Armenian meteorological stations were used. The research covers the year 2021 to be in line with satellite-based precipitation product quality and completeness (e.g., CMORPH and IMERG). The stations were chosen based on data completeness, spatial coverage, and elevation gradient. Daily precipitation observations at the stations were totalled over ten-day (decadal) periods for use in SPI computation. The chosen stations, which characterize varied topographic conditions, were scattered across separate elevation zones as follows:

- Lowland and foothill stations located below 1000 m a.s.l. These lower elevation sites are more prone to severe droughts due to higher temperatures and lower precipitation amounts.

- Low-mountain stations (1000–1700 m a.s.l.). Stations at this elevation have relatively milder climatic conditions compared to the lowlands; with this level of elevation, they have relatively less rigorous climate conditions.
- Mid-mountain stations (1700–2500 m a.s.l.). These areas are characterized by higher levels of precipitation and a mix of forested and agricultural landscapes.
- High-mountain stations (>2500 m a.s.l.). Located in mountainous areas of Armenia, these stations experience cool and humid climates due to higher precipitation and low temperatures.

Having stations from all elevation belts across Armenia is essential in determining the ability of satellite-based products to capture precipitation variability and drought regimes in complex mountainous terrain. Differences in SPI among these elevation belts inform us about the function of altitude in drought intensity.

### 2.2.2. Satellite-based Precipitation Products

The CMORPH Climate Data Record (CDR) provides satellite-derived precipitation estimates obtained from microwave remote sensing, which are bias-corrected using ground-based measurements (Xie et al. 2017). These estimates are combined and interpolated in time using the Climate Prediction Center Morphing Technique (MORPH). In this study, CMORPH data with 8 km spatial and 30-minute temporal resolution were used. IMERG is a multi-satellite precipitation product from NASA, combining estimates from passive microwave and infrared sensors within the Global Precipitation Measurement (GPM) satellite constellation. Precipitation is computed using the Goddard Profiling Algorithm, intercalibrated to the GPM Combined Ku Radar-Radiometer Algorithm product, and merged into half-hourly  $0.1^\circ \times 0.1^\circ$  (~ 10 × 10 km) fields (Huffman et al. 2019). CMORPH and IMERG utilize different schemes for precipitation estimation over areas not directly observed by microwave sensors. For ground-observation consistency, satellite-retrieved precipitation on sub-hourly timescales was summed to daily totals. A summary of all datasets used in this study, including satellite-based and in-situ observations, is provided in Table 1.

Table 1. Summary of datasets used in this study.

Dataset/Product	Parameter	Spatial resolution	Temporal coverage	Time scale	Cloud cover	Data source
Ground stations	Precipitation	Point	2000–2021	Daily	N/A	Hydrometeorology and Monitoring Center of Armenia
CMORPH CDR	Precipitation	~8 km	2000–2021	30 minutes (aggregated to daily)	N/A	NOAA Climate Prediction Center
GPM IMERG	Precipitation	~10 km	2000–2021	30 minutes (aggregated to daily)	N/A	NASA GES DISC
Sentinel-2 L2A	NDVI, NDWI, NDMI	10–20 m	June 2021	5-day revisit	≤ 10%	Copernicus Open Access Hub
Landsat-8 OLI	NDVI, NDWI, NDMI	30 m	June 2021	16-day revisit	≤ 10%	USGS EarthExplorer

### 2.2.3. Vegetation and moisture indices

Sentinel-2 is a two Sentinel-2A and Sentinel-2B polar-orbiting satellite mission with the Multispectral Instrument (MSI) on board for each, recording imagery in 13 spectral bands. The MSI is an optical imaging-capable high-resolution sensor that supports various applications, including land cover classification, vegetation monitoring, monitoring of water quality, maritime surveillance, and emergency response. Sentinel-2 ranges from 10 m to 60 m, and the radiometric resolution is 12-bit, with an aggregate revisit time (ESA 2023).

Landsat-8, launched jointly by the U.S. Geological Survey and NASA, provides moderate-resolution images of the world's polar and terrestrial regions. Landsat-8 provides moderate-resolution imagery (15–100 m) of the Earth's terrestrial and polar regions. It carries two primary instruments: the Operational Land Imager (OLI), which captures visible, near-infrared, and shortwave infrared data at a 30 m spatial resolution (with panchromatic data at 15 m), and the Thermal Infrared Sensor (TIRS), which captures thermal data at 100 m resolution. Vegetation and moisture indices from Sentinel-2 and Landsat-8 surface reflectance products were generated to evaluate vegetation health and surface moisture dynamics in June 2021. Six cloud-free scenes per satellite, corresponding to three ten-day intervals: 1–10, 11–20, and 21–30 June, were selected. Indices were generated using standard spectral bands from established methodologies (Gao 1996; Wilson and Sader 2002). The equations and spectral band definitions used for each satellite sensor are presented in Table 2, where the indices are B4 (Red), B8 and B5 (NIR), B11 and B6 (SWIR).

**Table 2.** Vegetation and moisture indices derived from Sentinel-2 and Landsat-8 imagery. All values of the indices range from -1 to +1.

Data source	Index	Formula
Sentinel-2	NDVI	$(\text{NIR} - \text{RED}) / (\text{NIR} + \text{RED})$
	NDWI	$(\text{NIR} - \text{SWIR}) / (\text{NIR} + \text{SWIR})$
	NDMI	$(\text{NIR} - \text{SWIR}) / (\text{NIR} + \text{SWIR})$
Landsat-8	NDVI	$(\text{NIR} - \text{RED}) / (\text{NIR} + \text{RED})$
	NDWI	$(\text{NIR} - \text{SWIR}) / (\text{NIR} + \text{SWIR})$
	NDMI	$(\text{NIR} - \text{SWIR}) / (\text{NIR} + \text{SWIR})$

The NDVI utilizes the red and near-infrared (NIR) bands to quantify vegetation greenness and vigor, based on the principle that healthy vegetation reflects more NIR and absorbs more red light (Rouse et al. 1974). The NDWI employs the NIR and SWIR bands to assess vegetation water content and surface moisture variations (Gao 1996). The NDMI also uses NIR and SWIR bands to evaluate vegetation moisture content, exploiting the difference in reflectance caused by variations in leaf water content.

### 2.3. The Standardized Precipitation Index

The SPI is a widely used meteorological drought indicator due to its flexibility across timescales and spatial consistency, making it valuable for short- and long-term drought evaluation. Unlike indices requiring complex data, SPI relies solely on precipitation, simplifying computation.

In this study, precipitation probability density functions were modeled using the gamma distribution at a decadal timescale. Empirical cumulative distribution functions (CDFs) were then derived from the observed ten-day precipitation totals, rescaled, and transformed using the inverse normal function to obtain the cumulative probability distribution for SPI computation (Guttman 1999).

### 2.4. Evaluation metrics

Spatial resolution differences complicate direct comparison between precipitation products and station observations. The point-to-pixel approach was employed, whereby the gridded rain gauge measurements are matched with the precipitation data within corresponding grid cells (Nastos and Zerefos 2009; Tan and Duan 2017; Nojarov 2024). We used the nearest-neighbor method, assigning the station value to the satellite grid cell in which it was located. The SPI obtained has been evaluated from station and satellite observations rather than raw precipitation amounts because SPI normalizes for local climatology and variability and thus enables consistent assessment of precipitation variability and dryness conditions across regions with differing precipitation regimes. Using SPI reduces the effects of heavy precipitation events and inter-annual variations and provides a more consistent measure with which to evaluate the ability of the satellite products to simulate drought trends.

To determine the accuracy and error of the precipitation products with respect to the in-situ reference dataset, certain statistical parameters were used

**Table 3.** The list of statistical evaluation metrics.

Statistical metrics	Formulation
Pearson correlation coefficient ( $r$ )	$r = \frac{\sum_{i=1}^n (X_i - \underline{X})(Y_i - \underline{Y})}{\sqrt{\sum_{i=1}^n (X_i - \underline{X})^2} \sqrt{\sum_{i=1}^n (Y_i - \underline{Y})^2}}$
Root mean square error (RMSE)	$RMSE = \sqrt{\frac{\sum_{i=1}^n (X_i - Y_i)^2}{n}}$
Bias	$Bias = \frac{1}{n} \sum_{i=1}^n (X_i - Y_i)$
Mean absolute error (MAE)	$MAE = \frac{1}{n} \sum_{i=1}^n  X_i - Y_i $
Standard deviation (SD)	$SD = \sqrt{\frac{1}{n} \sum_{i=1}^n (X_i - \underline{X})^2}$

that include the root mean square error (RMSE), mean absolute error (MAE), Pearson correlation coefficient ( $r$ ), mean bias (Bias), and standard deviation (SD), which are listed in Table 3.

The correlation coefficient ( $r$ ) estimates the statistical relationship between the temporal and spatial patterns of the precipitation products and reference measurements. RMSE estimates the average magnitude of differences between reference and satellite data, while MAE estimates the average absolute difference regardless of direction. Bias shows whether the satellite-retrieved precipitation (or SPI) systematically overestimates or underestimates the observed values. SD measures data consistency and variability, and relative standard deviation shows whether the satellite product over- or underestimates variability.

Where  $X_i$  is the SPI from satellite data,  $Y_i$  is the SPI from station observations, while  $\bar{X}$  and  $\bar{Y}$  are the means of the satellite and observed SPI, respectively. These statistics evaluate the performance and reliability of satellite-derived SPI by assessing its agreement with observed SPI values.

### 3. Results

#### 3.1. Analysis of meteorological droughts over Armenia in June 2021

The intensity and spatial distribution of meteorological droughts across Armenia in June 2021 were evaluated using the SPI. As illustrated in Fig. 3, extreme drought conditions prevailed over most parts of the country, indicating a substantial precipitation deficit during the study period. In contrast, the northeastern regions experienced relatively moderate conditions, where mild to near-normal drought categories were predominantly observed.

A ten-day (decadal) SPI for June 2021 evaluates the performance and reliability of satellite-retrieved precipitation datasets over the varied topography of Armenia. Fig. 4A–I provides graphical representations of the comparison results, presenting a clear, side-by-side comparison of satellite-retrieved and in-situ SPI for every ten days.

For clarity, the panels in Fig. 4 are organized as follows: Fig. 4A–C represent in-situ observations for decades 1, 2, and 3; Fig. 4D–F represent CMORPH; and Fig. 4G–I represent IMERG.

Fig. 4A–C show near-normal to dry conditions around Sevan Lake, Lori, Tavush, Shirak, and Armavir (SPI  $\sim -0.5$  to 0) during the first ten days (Fig. 4A), while the rest of the country experienced near-normal to wetter conditions (SPI  $> 0$ ). In the second ten-day interval (Fig. 4B), drought affected nearly 78% of the area. By the third ten-day period (Fig. 4C), moderate drought (SPI  $-1$  to  $-0.6$ ) was concentrated in the Ararat Valley, Shirak, Lori, Tavush, and the Sevan Lake region; the remaining areas experienced near-normal conditions (SPI  $> 0$ ).

Similarly, SPI from CMORPH (Fig. 4D–F) shows that during the first ten days (Fig. 4D), the southern regions were dry to normal (SPI  $-0.5$  to 0, near normal) and the northern regions were wetter than normal (SPI  $> 0$ , near normal to wet). In the second ten-day interval (Fig. 4E), drought was more extensive compared to the first or third decades, and SPI was below  $-1$  near Sevan Lake (moderate to severe drought). In the third ten-day interval (Fig. 4F), SPI in Ararat Valley was

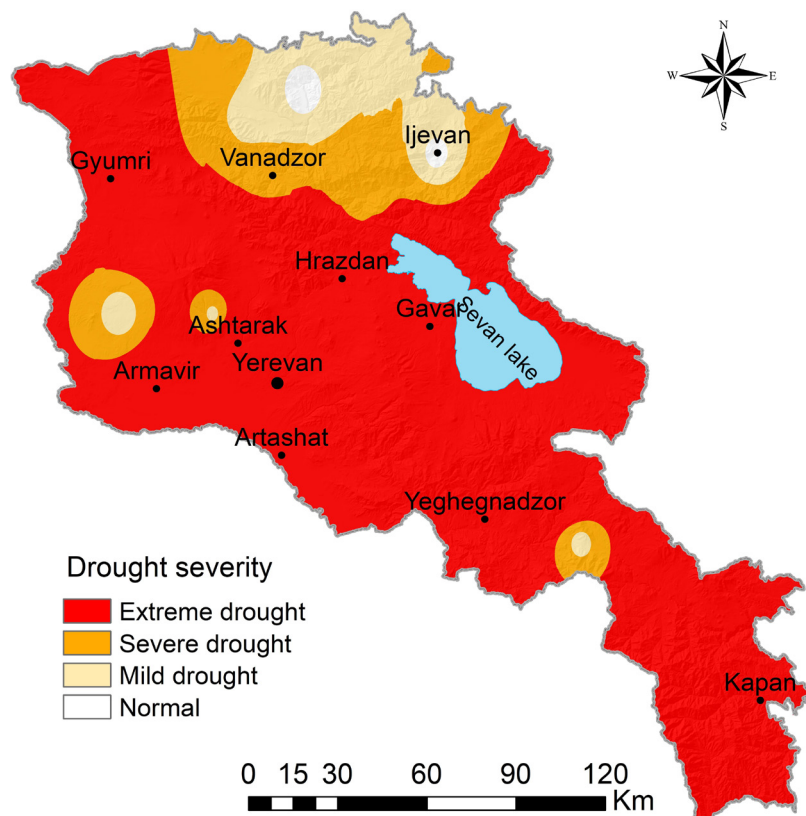


**Figure 3.** The severity of drought conditions over Armenia in June 2021, based on SPI and in-situ observations.

under  $-1$  to  $-0.6$  (moderate drought), whereas other regions were under SPI values above  $0$  (near normal to wet).

According to the IMERG-derived SPI (Fig. 4G–I), the drought condition in Armenia had perceivable spatial and temporal differences in June 2021. During the first ten-day period (Fig. 4G), almost 80% of Armenia experienced moderate to extreme drought ( $SPI < -1$ ), most severely affected by Ararat Valley, Syunik, Vayots Dzor, and Kotayk. In the second ten-day interval (Fig. 4K), the majority of the drought was confined to the Lori and Tavush regions ( $SPI$  between  $0.6$  and  $-1$ ), and other regions saw a recovery to normal ( $SPI \approx 0$ ). By the third ten-day period (Fig. 4I), most of Armenia was dominated by close to normal to slightly dry conditions, with moderate dryness in the Ararat Valley, Ashtarak area, and sections of Armavir and Kotayk ( $SPI$  from  $0.6$  to  $-1$ ), while Shirak, Vayots Dzor, and Syunik remained close to normal ( $SPI \approx 0$  to  $-0.5$ ), and Lake Sevan and Lori showed slightly wet conditions ( $SPI > 0$ ).

Generally, the SPI based on IMERG implies a gradual reduction of drought intensity from early to late June, in evidence of a shift from widespread dryness towards more normal moisture by the end of the month.

Overall, all three datasets reflect a uniform spatial pattern: drier in central Armenia (especially in the Ararat Valley) and wetter to the north and north-east. Observations provide the best local distribution, CMORPH overestimates somewhat in mountains, and IMERG has values close to observations but can sometimes underestimate local extremes. Overall, June 2021 was close to normal precipitation-wise, with no intense rainfalls or severe droughts.

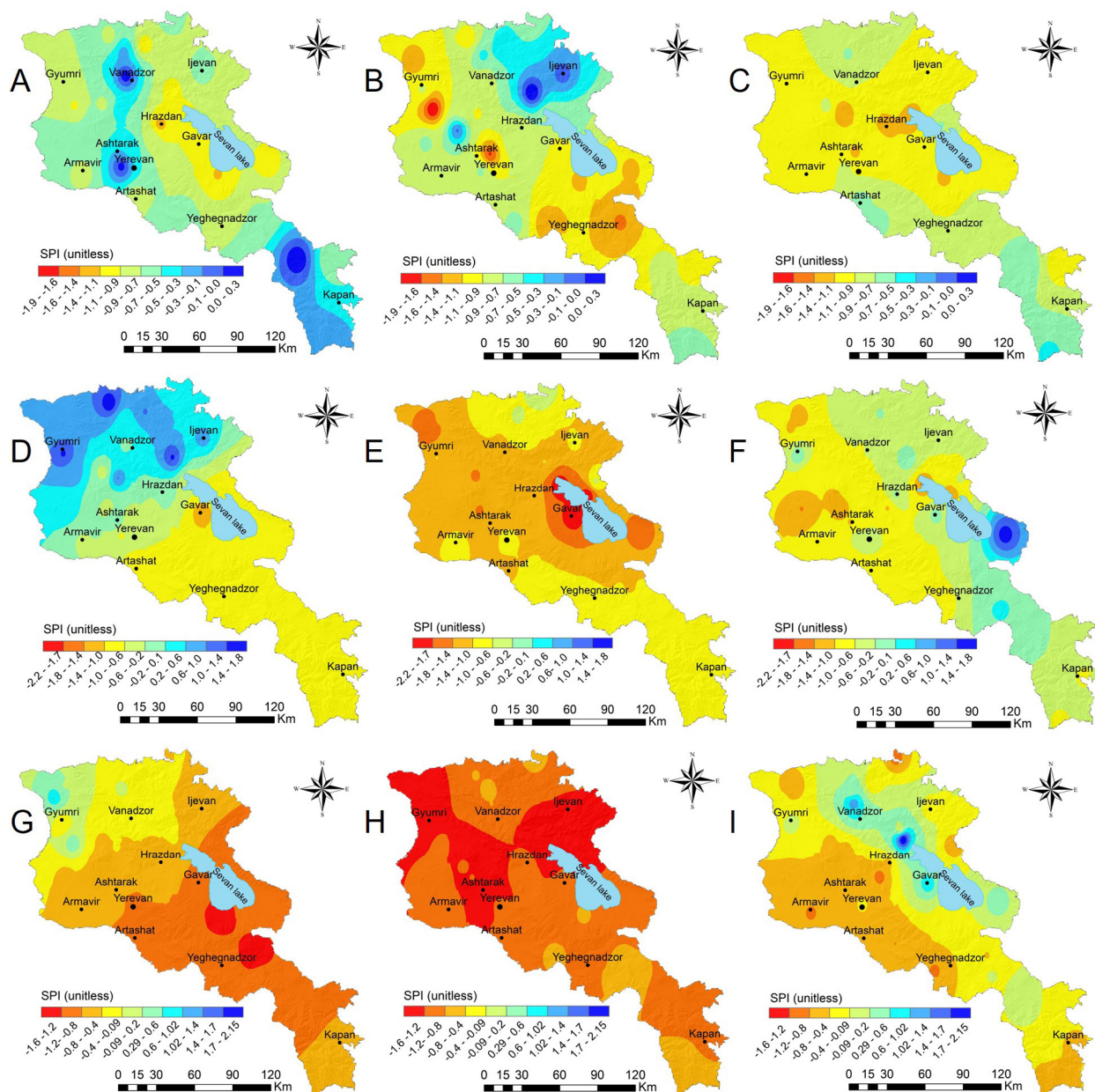


**Figure 4.** A ten-day SPI for June 2021. **A** in-situ observations for 1–10 June 2021 **B** in-situ observations for 11–20 June 2021 **C** in-situ observations for 21–30 June 2021 **D** CMORPH for 1–10 June 2021 **E** CMORPH for 11–20 June 2021 **F** CMORPH for 21–30 June 2021 **G** IMERG for 1–10 June 2021 **H** IMERG for 11–20 June 2021 **I** IMERG for 21–30 June 2021.

### 3.2. Analysis of drought conditions by the elevation zones

Fig. 5A–C illustrate the boxplot of ten-day SPI values by the four elevation zones according to in-situ observation and CMORPH and IMERG datasets in June 2021.

IMERG and CMORPH tend to overestimate SPI versus observations during the first decade (Fig. 5A). However, IMERG performs better, providing a more accurate representation of the mean (median SPI) and spatial variability (inter-quartile range) of drought conditions over Armenia. During the second decade (10–20 June) the worst performance was obtained for the third decade of June, when both IMERG and CMORPH significantly overestimate SPI failing to reproduce se-

vere drought conditions observed by in-situ observations (Fig. 5C). Overall, the satellite observations show poorer performance at higher elevated zones, between 1000 and 2000 m a.s.l., which is likely due to inadequate representation of orographic precipitation which are highly localised in summer (Gevorgyan 2018).

Table 4 shows the significant statistical parameters-correlation coefficient (R), RMSE, Bias, MAE, index of agreement (d), and relative standard deviation error (SD) to assess the satellite-based precipitation products (SbPPs) performance in comparison to ground measurements.

CMORPH and IMERG correlate relatively poorly with in-situ measurements, with Pearson  $r$  ranging from  $-0.08$  to  $0.41$  and  $0.01$  to  $0.28$ , respectively. Satellite-derived SPI and observed SPI correlation vary from weak positive to negative by decade, showing the poor consistency and limitations of satellite-based SPI estimation during this period.

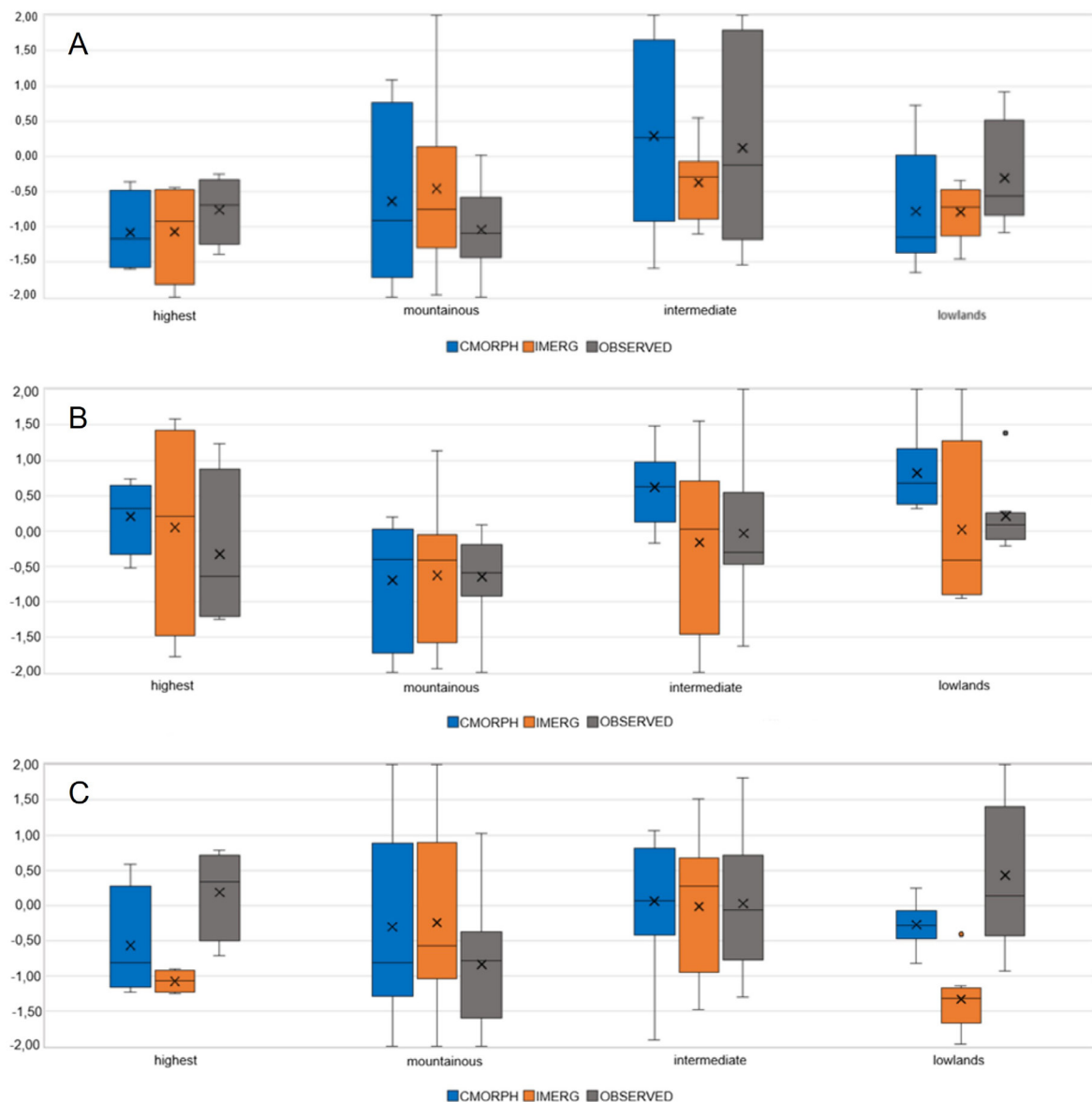


**Figure 5.** The boxplots for SPI values from the CMORPH (blue), IMERG (orange), and in-situ (grey) observations in June 2021. **A** June 1–10 **B** June 11–20 **C** June 21–30.

SPI will capture extreme wet and dry anomalies with a non-linear distribution. The traditional linear statistics of  $r$  and  $r^2$  may not be able to represent the satellite dataset’s depiction of extreme events, as these statistics are more sensitive to the central tendencies of data. RMSE quantifies differences between observed and satellite-based SPI values that vary between 0.56 and 1.48 for CMORPH and between 0.53 and 0.86 for IMERG. The closer the agreement is, the smaller the RMSE values are, and the lower IMERG RMSEs reveal that it estimates observed SPI better during most periods.

**Table 4.** Comparison of drought indices for the three decades of June.

	CMORPH (SPI)			IMERG (SPI)		
	1–10	11–20	21–30	1–10	11–20	21–30
Decades	1–10	11–20	21–30	1–10	11–20	21–30
$r$	0.41	0.23	-0.08	0.28	-0.05	0.01
RMSE	0.98	0.56	1.48	0.53	0.54	0.86
Bias	0.19	1.24	0.32	0.87	1.23	0.31
MAE	0.68	0.43	0.72	0.38	0.41	0.68
$d$	0.46	0.44	0.12	0.52	0.37	0.27
SD	0.85	0.43	1.28	0.48	0.27	0.48

MAE is the average error size regardless of direction. IMERG has a more petite MAE than CMORPH, particularly in the first (0.38) and the second (0.41) ten-day periods, which means more prediction accuracy. The agreement index ( $d$ ) quantifies the extent to which predicted values are close to observations. IMERG agrees slightly more with the first period than CMORPH, whereas both datasets concur similarly with the second. For both datasets, agreement falls in the third period, with CMORPH having a very low index of 0.12, showing less reliability for representing SPI variations in this period.

Table 5 displays relative SD errors of estimated SPI values and those calculated from CMORPH and IMERG for three ten-day periods. The measure indicates the extent to which variability of SPI is captured in each satellite product relative to ground observations.

Overall, relative SD errors in IMERG are minorer than in CMORPH, particularly for the first (1–10 days) and second (10–20 days) ten-day intervals, meaning that it better replicates the observed variation at the beginning and middle of June. Both data sets possess considerably larger relative errors for the third ten-day period (20–30 days), with CMORPH exhibiting the most significant deviation. This decline in performance indicates that neither dataset is a good representation of SPI variability in late June, pointing toward potential limitations in the satellite retrieval algorithms or regional atmospheric conditions for accuracy.

**Table 5.** Relative SD error (%) between satellite-derived and observed SPI values.

Dataset	1–10 June	11–20 June	21–30 June
CMORPH	124%	25%	256%
IMERG	26%	53%	33%

The Taylor diagram (Fig. 6) summarizes the key statistical metrics of  $r$ , SD, and RMSE. The Taylor diagram reveals that the performance of IMERG and CMORPH was different during June due to differences in precipitation patterns and the severity of the drought. During the first ten days, both datasets captured overall trends well enough, with CMORPH displaying greater spatial variability. During the second ten-day period, severe drought resulted in CMORPH overestimating variability, whereas observed IMERG reasonably well captured SPI with minimal spatial variation smoothing. During the third period, both data sets underestimated local droughts poorly, with CMORPH generating extreme variability errors and IMERG minimizing extremes. This variability suggests that the datasets are more suitable for short-term SPI monitoring rather than longer durations, helping assess their reliability for drought monitoring in specific periods.

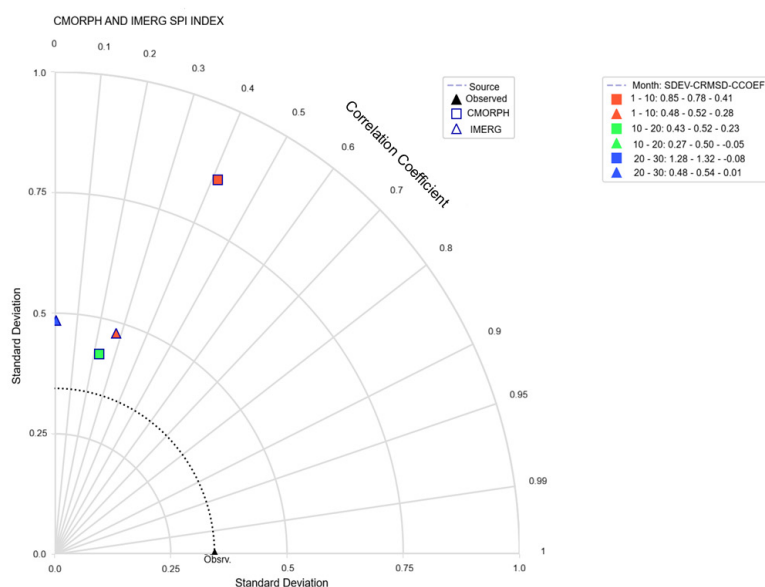


**Figure 6.** Taylor diagram comparing CMORPH, IMERG, and observed precipitation at 32 stations for the three ten-day periods of June 2021.

CMORPH slightly overestimated SPI in the first decade (bias 0.19) with moderate correlation (0.41) and high RMSE (0.98). Performance declined in the second (bias 1.24, low correlation 0.23, RMSE 0.56) and third decades (bias 0.32, negative correlation  $-0.08$ , RMSE 1.48). IMERG performed best in the first decade (bias 0.87, highest correlation, low RMSE), worsened in the second (bias 1.23, negative correlation, medium RMSE), and partially improved in the third (bias 0.31, near-zero correlation, highest RMSE). Both datasets have systematic overestimation, with higher consistency by IMERG across decades. Given its importance, detailed results are examined for five Ararat Valley stations: Yerevan-agro, Yerevan Zvartnots, Armavir, Artashat, and Ararat. The mean values of SPI by three decades are presented in Table 6.

CMORPH and IMERG show comparable trends across the three periods, with IMERG always recording lower SPI values than CMORPH. The SPI values recorded are generally more negative than those of CMORPH. However, they are closer to IMERG and suggest that IMERG will better represent the drought con-

**Table 6.** SPI comparison for Ararat Valley (June periods).

Period	CMORPH	IMERG	Observations
June 1–10	-0.69	-0.87	-0.81
June 11–20	-0.93	-1.16	-0.81
June 21–30	-0.67	-0.74	-0.86

ditions in the Ararat Valley. Based on the data noted, the driest periods are June 11–20 and June 21–30, with an SPI of  $-0.88$ . This shows persistent dryness for the second half of June. In addition, while both CMORPH and IMERG show the same tendency, their deviations from observed values confirm potential satellite-based estimation biases.

IMERG is more similar to observations, while CMORPH shows slightly less dryness. IMERG's lower values are identical to CMORPH, which suggests that IMERG can be more sensitive to dry spell detection. The drought indices calculated from the time series of Sentinel-2 and Landsat-8 show good results. NDVI, NDMI, and NDWI values range from  $-1$  to  $+1$  for both satellites in each decade. Overall, the NDVI from Sentinel-2 is reasonable, reflecting the variation in vegetation across Armenia, from arid to green zones (Fig. 7).

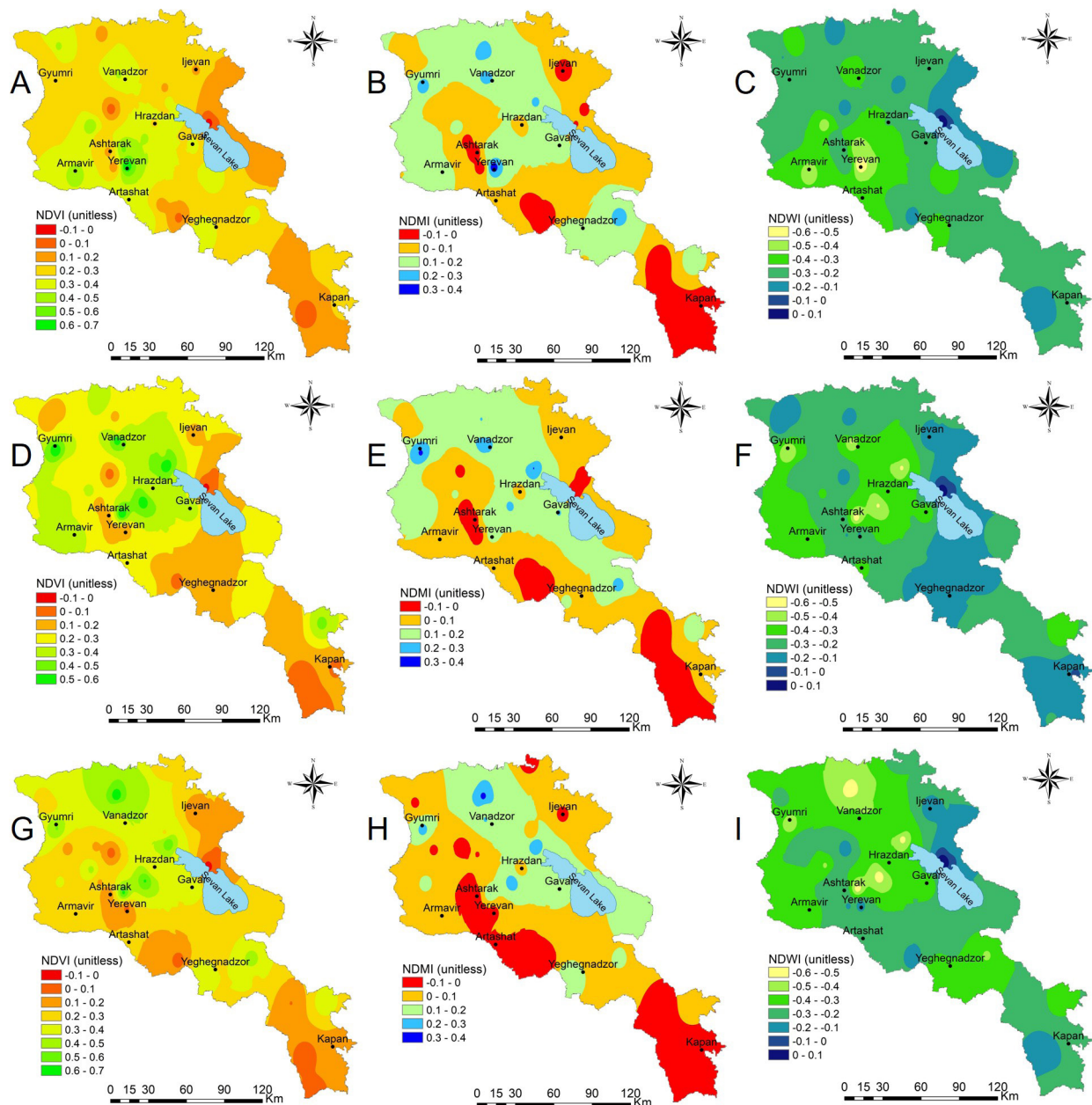
### 3.3. Vegetation and moisture indices

Fig. 7 presents the comparison of drought indices (NDVI, NDMI, NDWI) derived from Sentinel-2 for identical time intervals in June 2021. The maps show mean values for three ten-day periods (1–10, 11–20, and 21–30 June). For each period, decadal composites were produced by computing the pixel-wise median of all available cloud-free images, reducing cloud contamination and providing representative vegetation and moisture conditions, enabling a consistent temporal comparison between the two satellite datasets.

The evaluation shows that vegetation is denser at mid-to-high elevations, such as Egvard (0.52), Vanadzor (0.41), and Jermuk (0.33), while lower elevations, such as Meghri (0.06) and Aparan (0.05), have lower NDVI values. There is more moisture content (NDMI) in mountainous and forest regions, such as Gyumri (0.24) and Stepanavan (0.26), whereas dryness occurs in plains and valleys, such as Meghri ( $-0.06$ ) and Urtsadzor ( $-0.06$ ). Water presence (NDWI) is more negative in arid regions, i.e., Yerevan Arabkir ( $-0.61$ ) and Armavir ( $-0.44$ ), which are typically arid. Sevan Lake (0.07) has predicted greater NDWI values by its water content (Fig. 7A–C).

Fig. 7D–F presents high NDVI (0.57, 0.58, 0.58, and 0.60) and NDMI ( $-0.51$ ,  $-0.51$ ,  $-0.51$ , and  $-0.55$ ) values in areas like Gyumri, Vanadzor, Semyonovka, and Egvard. In contrast, regions such as Meghri, Kajaran, Ananun Canyon, and Aparan display low NDVI values (0.07, 0.06, 0.07, and 0.05) along with low NDMI values ( $-0.07$ ,  $-0.09$ ,  $-0.08$ , and 0.02), suggesting arid conditions with sparse vegetation. Sevan Lake and Shorja show relatively higher NDWI values ( $-0.31$  and 0.06, respectively), which indicate potential water presence, while Yeghvard ( $-0.55$ ), Fantan ( $-0.51$ ), and Gyumri ( $-0.50$ ) exhibit the driest conditions.

Key findings for the 21–30-day period are indicated in Fig. 7G–I. Mountainous and forested areas show high NDVI (0.67, 0.59, 0.39, and 0.51, respective-



**Figure 7.** Comparison of drought indices (NDVI, NDMI, NDWI) derived from Sentinel-2 for three June 2021 periods. **A** NDVI for 1–10 June 2021 **B** NDMI for 1–10 June 2021 **C** NDWI for 1–10 June 2021 **D** NDVI for 11–20 June 2021 **E** NDMI for 11–20 June 2021 **F** NDWI for 11–20 June 2021 **G** NDVI for 21–30 June 2021 **H** NDMI for 21–30 June 2021 **I** NDWI for 21–30 June 2021.

ly) and NDMI (0.32, 0.29, 0.20, and 0.23) values, indicating lush vegetation with good moisture content. Urban and semi-arid areas, including Yerevan, Meghri, and Kapan, show lower NDVI (0.08, 0.08, and 0.16) and NDMI (−0.03, −0.07, and −0.11) values. NDWI is consistently negative, indicating little surface water presence, except for a slightly positive value in Shorja (0.09), which may indicate a wetland or nearby water body.

The result from Landsat-8 for the period 1–10 June 2021 (Fig. 8) shows that high vegetation (NDVI) is observed in Gavar (0.47) and Gyumri (0.47), while Talin (−0.02) and Amberd (0.06) have minimal vegetation. Moisture (NDMI) is highest in Gyumri (0.25), Gavar (0.25), and Sevan Lake (0.23), while drier con-

ditions are seen in Talin (0.05) and Amberd (-0.05). Negative values of water presence (NDWI) indicate dry areas, with Gyumri (-0.43), Gavar (-0.43), and Sevan Lake (-0.40) being the driest. Jermuk (0.01) and Ararat (-0.15) show slightly better water presence.

Thus, based on the analysis of vegetation and moisture indices (NDVI, NDMI, NDWI) derived from Landsat-8 data, the following findings can be made:

- Higher elevations tend to have better vegetation and moisture.
- Moisture availability varies significantly, influencing vegetation health.
- Most areas show negative NDWI values, indicating limited water presence.

For 11–20 June 2021 (Fig. 8), NDVI values indicated dense vegetation in the northeastern and southern agricultural zones (e.g., Bagratashen, Kajaran,

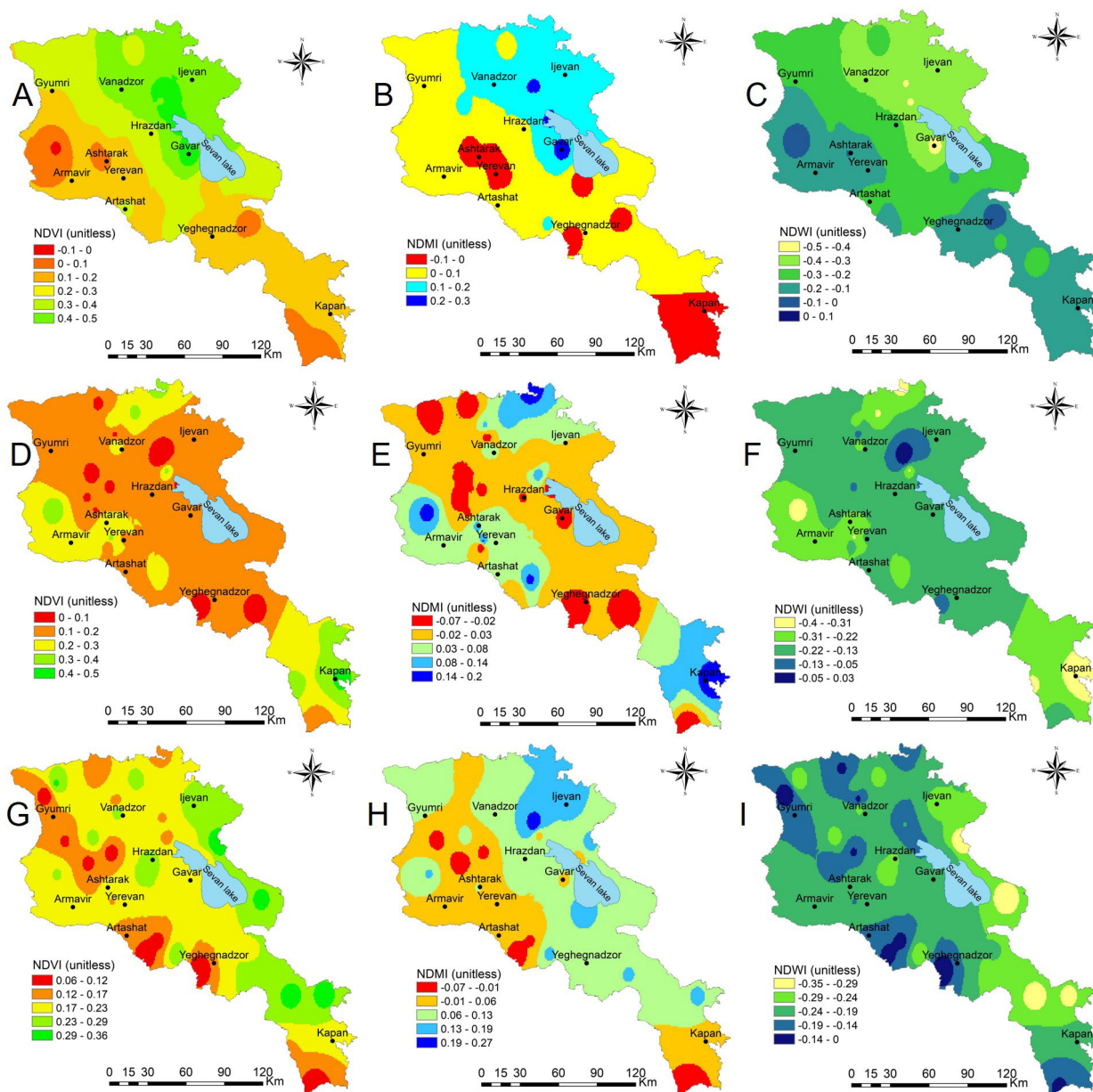


**Figure 8.** Comparison of drought indices (NDVI, NDMI, NDWI) derived from Landsat-8 for three June 2021 periods. **A** NDVI for 1–10 June 2021 **B** NDMI for 1–10 June 2021 **C** NDWI for 1–10 June 2021 **D** NDVI for 11–20 June 2021 **E** NDMI for 11–20 June 2021 **F** NDWI for 11–20 June 2021 **G** NDVI for 21–30 June 2021 **H** NDMI for 21–30 June 2021 **I** NDWI for 21–30 June 2021.

Yerevan-agro), while much lower values in areas such as Gyumri and Dilijan reflected sparse vegetation cover. The results show higher vegetation moisture in Bagratashen, Kapan, and Talin, and drier conditions in high-altitude regions like Aragats and Ashotsk. At the same time, mountainous and urbanized areas exhibited lower vegetation density and moisture, mainly due to terrain, precipitation gradients, and land use.

During 21–30 June 2021, NDVI values indicated relatively healthy vegetation in highland and forested zones such as Tchambarak, Sisian, and Goris (0.30–0.36), while very low values in the Ararat Valley and southern regions (e.g., Areni, Meghri, Ararat, ~0.06–0.08) reflected stressed or sparse vegetation. NDMI results show increased vegetation wetness in Dilijan, Gyumri, and Martuni, and much drier conditions in Aragats, Artik, and Meghri. NDWI values confirmed the contrast: fertile valleys and irrigated terrain experienced limited surface water availability, while mountainous and forest regions possessed relatively greater wetness. Overall, the Ararat Valley consistently exhibited low NDVI, negative NDMI, and negative NDWI values, and it was vulnerable to drought and dependence on irrigation. These observations emphasize how water stress is a chronic condition in semi-arid lowlands, while moisture is more abundant in mountainous and forested areas.

#### 4. Discussion

The suggested methodological innovation combines multi-source precipitation products (IMERG, CMORPH), SPI analysis, and vegetation indices (NDVI). An example of the research location was the spatiotemporal patterns of drought in the mountain regions of Armenia. The primary objective was to investigate the performance of satellite rainfall data in tracking the conditions of drought and combining them with in-situ measurements and vegetation indices to obtain meteorological and ecological characteristics of drought. Although such multi-source approaches were used elsewhere (Shayeghi et al. 2024), they are not used in complex areas, e.g., in Armenia. This emphasizes a methodological lacuna, given that the majority of previous research has been conducted on flat or arid areas as opposed to mountainous terrain.

To start with, the difference between SPI based on CMORPH and IMERG shows that both satellite records track drought variability in general agreement with ground data, but carry some differences in intensity and timing. Similar comparisons between IMERG and CMORPH have shown that IMERG is prone to provide higher accuracy (Derin et al. 2016; Nojarov et al. 2023) due to its use of the GPM core observatory's Dual-frequency Radar for calibration, which improves detection in complex terrain, and a more advanced scheme for integrating infrared data, leading to better spatial representation of precipitation. Despite these limitations, IMERG and CMORPH were also found to remain suitable for drought monitoring in data-scarce mountainous regions.

Second, the application of NDVI (along with associated indices NDMI and NDWI) is a reflection of interactions between vegetation response and meteorological drought. Here, the lag in SPI anomalies as well as in the indicators of vegetation stress is in line with other studies carried out in Mediterranean and Central Asian contexts, where vegetation reacts with a lag behind moisture deficiency (Sahoo et al. 2015; Papagiannopoulou et al. 2017). This lag emphasizes the merit

of integrating ecological and meteorological indices because vegetation-based observations may underestimate the beginning of early droughts but provide more information about ecosystem recovery and resilience (Vicente-Serrano et al. 2013). Therefore, the combined SPI–NDVI analysis reveals more insight into the propagation of the drought from atmospheric to landscape-scale impacts.

Third, the integration of ground observation, satellite precipitation, and vegetation indices improves the estimation of drought duration, intensity, and spatial coverage. Other integration methods have been seen to improve the accuracy of drought detection for regions that do not have a dense network of observations (Pozzi et al. 2013; Naumann et al. 2018). Particularly, studies have shown that the combination of meteorological and ecological indicators allows for a better description of short-term atmospheric anomalies and long-term ecosystem impacts (Vogel et al. 2021). That our findings are in accordance with these is an indication that the multi-source approach employed herein can be extended for operational drought monitoring across mountainous or data-constrained areas. This is a demonstration of its possibilities for application to larger areas of regions with similar topographical and climatic limitations.

Finally, while SPI and vegetation indices provide good data on meteorological and ecological drought, they fail to quantify fully socio-economic impacts, as noted by Wilhite and Pulwarty (2017) in proposing the inclusion of impact-based indicators of drought in monitoring schemes. Furthermore, since CMORPH and IMERG data are being updated day in and day out, future studies should incorporate larger time series and other such indices as soil moisture and evapotranspiration, in accordance with recommendations by Hao et al. (2018) for more comprehensive drought research. Despite these limitations, the simplicity and scalability of the proposed framework make it consistent with previous efforts to develop transferable drought monitoring systems for high-relief or data-scarce environments (Derin et al. 2016). Hence, the methodology presented above provides a practical foundation for enhanced drought resilience in compound terrains.

## 5. Conclusion

This study evaluated the performance of satellite precipitation data from CMORPH and IMERG for estimating the SPI in the mountainous regions of Armenia during June 2021 by integrating these data with in-situ observations and vegetation indices (NDVI, NDMI, NDWI). The results reported dominant patterns in drought duration, intensity, and spatial distributions and indicated that IMERG tends to be more accurate compared to CMORPH in short-term decadal SPI estimates, particularly in lower and mid-mountain elevation zones.

One of the main contributions of this research is the merging of multi-source satellite precipitation and ecological indicators, making it possible to evaluate meteorological and ecological drought severity simultaneously. This made it possible to conclude that highland areas had higher vegetation moisture and NDVI values, while lowlands such as the Ararat Valley experienced constant dryness, which is reflective of elevation-dependent drought vulnerability. These findings are in agreement with other semi-arid and mountainous regions' reports (Sahoo et al. 2015; Papagiannopoulou et al. 2017) but widen the research to cover Armenia, a region that has been under drought research in the world.

The study also presented the capability of satellite-derived SPI in detecting general drought trends, but with less capability to reflect intense local occurrences, particularly over terrain that is mountainous. Biases in CMORPH and IMERG observed in this study are reflective of topographic challenges, which can be delivered through the data cube platform and cloud services (Astsatryan et al. 2015, 2018, 2022). The inability aside, the combination of satellite precipitation with vegetation indices enables a more holistic and operationally useful depiction of drought, supporting early warning, irrigation planning, and climate-resilient water management in data-scarce mountainous areas.

Finally, while the analysis was limited to a single month, June 2021, the results lay out a template for upscaling this method to longer time periods and other mountainous regions, adding additional indicators such as soil moisture, evapotranspiration, and socio-economic impacts. This study defines the potential of multi-source Earth observation data in enabling drought monitoring and resilience planning for regions with limited ground-based observations.

## References

- Abrahamyan R, Astsatryan H, Grigoryan H, Sahakyan V (2023) Cloud infrastructure environment based on data cube and machine learning technologies. In: Shoukourian Y, Dayde M (Eds) Proceedings of the 1st International Conference on Frontiers of Digital Technology Towards a Sustainable Society, Yerevan (Armenia). AIP Conference Proceedings 2757(1): 030001. <https://doi.org/10.1063/5.0136314>
- Adler C, Wester P, Bhatt I, Huggel C, Insarov GE, Morecroft MD, Muccione V, Prakash A (2022) Cross-Chapter Paper 5: Mountains. In: Pörtner H-O, Roberts DC, Tignor M, Poloczanska ES, Mintenbeck K, Alegría A, Craig M, Langsdorf S, Lösschke S, Möller V, Okem A, Rama B (Eds) Climate Change 2022: Impacts, Adaptation and Vulnerability. Contribution of Working Group II to the Sixth Assessment Report of the Intergovernmental Panel on Climate Change. Cambridge University Press, Cambridge, UK and New York, NY, USA, 2273–2318. <https://doi.org/10.1017/9781009325844.022>
- Ageet S, Fink AH, Maranan M, Diem JE, Hartter J, Ssali AL, Ayabagabo P (2022) Validation of Satellite Rainfall Estimates over Equatorial East Africa. *Journal of Hydrometeorology* 23(2): 129–151. <https://doi.org/10.1175/JHM-D-21-0145.1>
- Ahmadalipour A, Moradkhani H (2018) Multi-dimensional assessment of drought vulnerability in Africa: 1960–2100. *Science of The Total Environment* 644: 520–535. <https://doi.org/10.1016/j.scitotenv.2018.07.023>
- Astsatryan H, Grigoryan H, Abrahamyan R, Asmaryan S, Muradyan V, Tepanosyan G, Guigoz Y, Giuliani G (2022) Shoreline delineation service: using an earth observation data cube and Sentinel 2 images for coastal monitoring. *Earth Science Informatics* 15(3): 1587–1596. <https://doi.org/10.1007/s12145-022-00806-7>
- Astsatryan H, Grigoryan H, Poghosyan A, Abrahamyan R, Asmaryan S, Muradyan V, Tepanosyan G, Guigoz Y, Giuliani G (2021) Air temperature forecasting using artificial neural network for Ararat valley. *Earth Science Informatics* 14(2): 711–722. <https://doi.org/10.1007/s12145-021-00583-9>
- Astsatryan H, Grogoryan H, Gyulgyulyan E, Hakobyan A, Kocharyan A, Narsisian W, Sahakyan V, Shoukourian Y, Abrahamyan R, Petrosyan Z, Aligon J (2018) Weather Data Visualization and Analytical Platform. *Scalable Computing: Practice and Experience* 19(2): 79–86. <https://doi.org/10.12694/scpe.v19i2.1351>

- Astsatryan H, Hayrapetyan A, Narsisian W, Saribekyan A, Asmaryan Sh, Saghatelyan A, Muradyan V, Guigoz Y, Giuliani G, Ray N (2015) An interoperable web portal for parallel geoprocessing of satellite image vegetation indices. *Earth Science Informatics* 8(2): 453–460. <https://doi.org/10.1007/s12145-014-0165-3>
- Azizyan HH, Panyan HS, Gevorgyan AM, Khalatyan YS, Gizhlaryan SH, Astsatryan HV, Sahakyan VG, Azizyan LV (2023) Analysis of drought conditions in Armenia in June 2021 using observational and satellite data. *Proceedings of the YSU C: Geological and Geographical Sciences* 57(3): 163–169. <https://doi.org/10.46991/PYSU:C/2023.57.3.163>
- Derin Y, Anagnostou E, Berne A, Borga M, Boudevillain B, Buytaert W, Chang C-H, Delrieu G, Hong Y, Hsu YC, Lavado-Casimiro W, Manz B, Moges S, Nikolopoulos EI, Sahlü D, Salerno F, Rodríguez-Sánchez J-P, Vergara HJ, Yilmaz KK (2016) Multiregional Satellite Precipitation Products Evaluation over Complex Terrain. *Journal of Hydrometeorology* 17(6): 1817–1836. <https://doi.org/10.1175/JHM-D-15-0197.1>
- Duan Z, Liu J, Tuo Y, Chiogna G, Disse M (2016) Evaluation of eight high spatial resolution gridded precipitation products in Adige Basin (Italy) at multiple temporal and spatial scales. *Science of The Total Environment* 573: 1536–1553. <https://doi.org/10.1016/j.scitotenv.2016.08.213>
- Sahoo RN, Dutta D, Khanna M, Kumar N, Bandyopadhyay SK (2015) Drought assessment in the Dhar and Mewat Districts of India using meteorological, hydrological and remote-sensing derived indices. *Natural Hazards* 77(2): 733–751. <https://doi.org/10.1007/s11069-015-1623-z>
- Easterling DR, Wallis TWR, Lawrimore JH, Heim RR (2007) Effects of temperature and precipitation trends on U.S. drought. *Geophysical Research Letters* 34(20): 2007GL031541. <https://doi.org/10.1029/2007GL031541>
- ESA [European Space Agency] (2023) Sentinel-2 Mission Overview [https://www.esa.int/Applications/Observing\\_the\\_Earth/Copernicus/Sentinel-2](https://www.esa.int/Applications/Observing_the_Earth/Copernicus/Sentinel-2) [Accessed on 10.02.2025]
- Gao B (1996) NDWI—A normalized difference water index for remote sensing of vegetation liquid water from space. *Remote Sensing of Environment* 58(3): 257–266. [https://doi.org/10.1016/S0034-4257\(96\)00067-3](https://doi.org/10.1016/S0034-4257(96)00067-3)
- Gevorgyan A (2013) Verification of daily precipitation amount forecasts in Armenia by ERA-Interim model. *International Journal of Climatology* 33(12): 2706–2712. <https://doi.org/10.1002/joc.3621>
- Gevorgyan A (2018) Convection-Permitting Simulation of a Heavy Rainfall Event in Armenia Using the WRF Model. *Journal of Geophysical Research: Atmospheres* 123(19): 11008–11029. <https://doi.org/10.1029/2017JD028247>
- Gevorgyan A, Piliposyan N, Gizhlaryan S, Sargsyan S (2025) Climate Change Impact on Extreme Temperatures and Heat Waves in Armenia. *International Journal of Climatology* 45(7): e8802. <https://doi.org/10.1002/joc.8802>
- Guttman NB (1999) Accepting the Standardized Precipitation Index: A Calculation Algorithm. *JAWRA Journal of the American Water Resources Association* 35(2): 311–322. <https://doi.org/10.1111/j.1752-1688.1999.tb03592.x>
- Hao Z, Singh VP, Xia Y (2018) Seasonal Drought Prediction: Advances, Challenges, and Future Prospects. *Reviews of Geophysics* 56(1): 108–141. <https://doi.org/10.1002/2016RG000549>
- Huffman GJ, Bolvin DT, Braithwaite D, Hsu K, Joyce R, Kidd C, Nelkin EJ, Sorooshian S, Tan J, Xie P (2019) NASA Global Precipitation Measurement (GPM) Integrated Multi-satellite Retrievals for GPM (IMERG). Algorithm Theoretical Basis Document (ATBD). Version 06. NASA. [https://gpm.nasa.gov/sites/default/files/document\\_files/IMERG\\_ATBD\\_V06.pdf](https://gpm.nasa.gov/sites/default/files/document_files/IMERG_ATBD_V06.pdf) [Accessed on 20.03.2025]

- Li Y, Yan H, Chen L, Huang M, Shou W, Zhu L, Zhao L, Xing Y (2024) Performance and uncertainties of five popular satellite-based precipitation products in drought monitoring for different climate regions. *Journal of Hydrology* 628: 130562. <https://doi.org/10.1016/j.jhydrol.2023.130562>
- Lu J, Jia L, Menenti M, Yan Y, Zheng C, Zhou J (2018) Performance of the Standardized Precipitation Index Based on the TMPA and CMORPH Precipitation Products for Drought Monitoring in China. *IEEE Journal of Selected Topics in Applied Earth Observations and Remote Sensing* 11(5): 1387–1396. <https://doi.org/10.1109/JSTARS.2018.2810163>
- Nastos PT, Zerefos CS (2009) Spatial and temporal variability of consecutive dry and wet days in Greece. *Atmospheric Research* 94(4): 616–628. <https://doi.org/10.1016/j.atmosres.2009.03.009>
- Naumann G, Alfieri L, Wyser K, Mentaschi L, Betts RA, Carrao H, Spinoni J, Vogt J, Feyen L (2018) Global Changes in Drought Conditions Under Different Levels of Warming. *Geophysical Research Letters* 45(7): 3285–3296. <https://doi.org/10.1002/2017GL076521>
- Nojarov P (2024) Evaporation and the difference between precipitation and evaporation in Bulgaria. *Journal of the Bulgarian Geographical Society* 51: 131–149. <https://doi.org/10.3897/jbgs.e135422>
- Nojarov P, Vlaskov V, Vatova Y (2023) Influence of atmospheric circulation on the spatial distribution of precipitation in the area of Sofia city. *Journal of the Bulgarian Geographical Society* 49: 17–25. <https://doi.org/10.3897/jbgs.e108747>
- Papagiannopoulou C, Miralles DG, Dorigo WA, Verhoest NEC, Depoorter M, Waegeman W (2017) Vegetation anomalies caused by antecedent precipitation in most of the world. *Environmental Research Letters* 12(7): 074016. <https://doi.org/10.1088/1748-9326/aa7145>
- Petrosyan D, Astsatryan H (2022) Serverless High-Performance Computing over Cloud. *Cybernetics and Information Technologies* 22(3): 82–92. <https://doi.org/10.2478/cait-2022-0029>
- Rouse JW Jr, Haas RH, Schell JA, Deering DW (1974) Monitoring vegetation systems in the Great Plains with ERTS. In: NASA Goddard Space Flight Center (Ed.), *Third Earth Resources Technology Satellite-1 Symposium 1*, NASA, Washington DC, 309–317.
- Pozzi W, Sheffield J, Stefanski R, Cripe D, Pulwarty R, Vogt JV, Heim RR, Brewer MJ, Svoboda M, Westerhoff R, Van Dijk AIJM, Lloyd-Hughes B, Pappenberger F, Werner M, Dutra E, Wetterhall F, Wagner W, Schubert S, Mo K, Nicholson M, Bettio L, Nunez L, Van Beek R, Bierkens M, De Goncalves LGG, De Mattos JGZ, Lawford R (2013) Toward Global Drought Early Warning Capability: Expanding International Cooperation for the Development of a Framework for Monitoring and Forecasting. *Bulletin of the American Meteorological Society* 94(6): 776–785. <https://doi.org/10.1175/BAMS-D-11-00176.1>
- Sen Roy S, Balling RC (2004) Trends in extreme daily precipitation indices in India. *International Journal of Climatology* 24(4): 457–466. <https://doi.org/10.1002/joc.995>
- Shayeghi A, Ziveh AR, Bakhtar A, Teymoori J, Hanel M, Vargas Godoy MR, Markonis Y, AghaKouchak A (2024) Assessing drought impacts on groundwater and agriculture in Iran using high-resolution precipitation and evapotranspiration products. *Journal of Hydrology* 631: 130828. <https://doi.org/10.1016/j.jhydrol.2024.130828>
- Shi S, Yao F, Zhang J, Yang S (2020) Evaluation of Temperature Vegetation Dryness Index on Drought Monitoring Over Eurasia. *IEEE Access* 8: 30050–30059. <https://doi.org/10.1109/ACCESS.2020.2972271>
- Spinoni J, Naumann G, Vogt JV (2017) Pan-European seasonal trends and recent changes of drought frequency and severity. *Global and Planetary Change* 148: 113–130. <https://doi.org/10.1016/j.gloplacha.2016.11.013>

- Sun Q, Miao C, Duan Q, Ashouri H, Sorooshian S, Hsu K (2018) A Review of Global Precipitation Data Sets: Data Sources, Estimation, and Intercomparisons. *Reviews of Geophysics* 56(1): 79–107. <https://doi.org/10.1002/2017RG000574>
- Tan M, Duan Z (2017) Assessment of GPM and TRMM Precipitation Products over Singapore. *Remote Sensing* 9(7): 720. <https://doi.org/10.3390/rs9070720>
- Tao H, Fischer T, Zeng Y, Fraedrich K (2016) Evaluation of TRMM 3B43 Precipitation Data for Drought Monitoring in Jiangsu Province, China. *Water* 8(6): 221. <https://doi.org/10.3390/w8060221>
- Toté C, Patricio D, Boogaard H, Van Der Wijngaart R, Tarnavsky E, Funk C (2015) Evaluation of Satellite Rainfall Estimates for Drought and Flood Monitoring in Mozambique. *Remote Sensing* 7(2): 1758–1776. <https://doi.org/10.3390/rs70201758>
- UNESCAP [United Nations Economic and Social Commission for Asia and the Pacific] (2020) Ready for the Dry Years: Building Resilience to Drought in South-East Asia - With a focus on Cambodia, Lao People's Democratic Republic, Myanmar and Viet Nam. United Nations. <https://doi.org/10.18356/9789210052771>
- Vicente-Serrano SM, Gouveia C, Camarero JJ, Beguería S, Trigo R, López-Moreno JI, Azorín-Molina C, Pasho E, Lorenzo-Lacruz J, Revuelto J, Morán-Tejeda E, Sanchez-Lorenzo A (2013) Response of vegetation to drought time-scales across global land biomes. *Proceedings of the National Academy of Sciences* 110(1): 52–57. <https://doi.org/10.1073/pnas.1207068110>
- Vogel J, Paton E, Aich V (2021) Seasonal ecosystem vulnerability to climatic anomalies in the Mediterranean. *Biogeosciences* 18(22): 5903–5927. <https://doi.org/10.5194/bg-18-5903-2021>
- Wang W, Ertsen MW, Svoboda MD, Hafeez M (2016) Propagation of Drought: From Meteorological Drought to Agricultural and Hydrological Drought. *Advances in Meteorology* 2016: 1–5. <https://doi.org/10.1155/2016/6547209>
- Wang X, Jiang D, Lang X (2017) Future extreme climate changes linked to global warming intensity. *Science Bulletin* 62(24): 1673–1680. <https://doi.org/10.1016/j.scib.2017.11.004>
- Wang YD, Chen H, Liu CR, Ding YJ (2018) Applicability of ITPCAS and CMORPH Precipitation Datasets over Shaanxi Province. *Arid Zone Research* 35(3): 579–588.
- Wilhite DA, Pulwarty RS (2017) Drought and Water Crises: Integrating Science, Management, and Policy. 2nd ed. Wilhite D, Pulwarty RS (Eds). CRC Press, 582 pp. <https://doi.org/10.1201/b22009>
- Wilson EH, Sader SA (2002) Detection of forest harvest type using multiple dates of Landsat TM imagery. *Remote Sensing of Environment* 80(3): 385–396. [https://doi.org/10.1016/S0034-4257\(01\)00318-2](https://doi.org/10.1016/S0034-4257(01)00318-2)
- World Bank Group, Asian Development Bank (2021) Climate Risk Country Profile: Armenia. World Bank Publications, The World Bank Group, Washington, DC, 28 pp.
- Wu J, Miao C, Zheng H, Duan Q, Lei X, Li H (2018) Meteorological and Hydrological Drought on the Loess Plateau, China: Evolutionary Characteristics, Impact, and Propagation. *Journal of Geophysical Research: Atmospheres* 123(20): 11569–11584. <https://doi.org/10.1029/2018JD029145>
- Xie P, Joyce R, Wu S, Yoo S-H, Yarosh Y, Sun F, Lin R (2017) Reprocessed, Bias-Corrected CMORPH Global High-Resolution Precipitation Estimates from 1998. *Journal of Hydro-meteorology* 18(6): 1617–1641. <https://doi.org/10.1175/JHM-D-16-0168.1>
- Xu SG, Niu Z, Shen Y, Kuang D (2014) A research into the characters of CMORPH remote sensing precipitation error in China. *Remote Sensing Technology and Applications* 29(2): 189–194.

- Yao J, Zhao Y, Chen Y, Yu X, Zhang R (2018) Multi-scale assessments of droughts: A case study in Xinjiang, China. *Science of The Total Environment* 630: 444–452. <https://doi.org/10.1016/j.scitotenv.2018.02.200>
- Zhang Q, Yu H, Sun P, Singh VP, Shi P (2019) Multisource data based agricultural drought monitoring and agricultural loss in China. *Global and Planetary Change* 172: 298–306. <https://doi.org/10.1016/j.gloplacha.2018.10.017>
- Zeweldi DA, Gebremichael M (2009) Evaluation of CMORPH Precipitation Products at Fine Space–Time Scales. *Journal of Hydrometeorology* 10(1): 300–307. <https://doi.org/10.1175/2008JHM1041.1>
- Zhong R, Chen X, Lai C, Wang Z, Lian Y, Yu H, Wu X (2019) Drought monitoring utility of satellite-based precipitation products across mainland China. *Journal of Hydrology* 568: 343–359. <https://doi.org/10.1016/j.jhydrol.2018.10.072>
- Zhu Q, Luo Y, Zhou D, Xu Y-P, Wang G, Gao H (2019) Drought Monitoring Utility using Satellite-Based Precipitation Products over the Xiang River Basin in China. *Remote Sensing* 11(12): 1483. <https://doi.org/10.3390/rs11121483>

## Additional information

### Conflict of interest

No conflict of interest was declared.

### Ethical statement

No ethical statement was reported.

### Use of AI

No use of AI was reported.

### Funding

The Science Committee of the Republic of Armenia supported the research in the frames of research project 21AG-1B052 and a Target project entitled “Creating a Cloud Computing Environment for Solving Scientific and Applied Problems” (№ 1-8/TB-23). The computational resources of the Armenian IaaS Cloud were utilized for conducting the experiments (Petrosyan and Astsatryan 2022; Abrahamyan et al. 2023)..

### Author contributions

Conceptualization: HA, FK. Data curation: RA. Formal analysis: AG, RA, HP. Methodology: AG, RA, HA. Project administration: HA. Resources: AG. Supervision: FK, HA. Validation: AG, RA, HP. Writing - review and editing: FK, AG, HA, HP, RA.

### Author ORCIDs

Hrachya Astsatryan  <https://orcid.org/0000-0001-8872-6620>

Rita Abrahamyan  <https://orcid.org/0000-0003-0009-8899>

Artur Gevorgyan  <https://orcid.org/0000-0003-1220-3617>

Hasmik Panyan  <https://orcid.org/0009-0009-7830-6679>

Furtado Kalli  <https://orcid.org/0000-0002-5166-112X>

### Data availability

All of the data that support the findings of this study are available in the main text or Supplementary Information.